INSTITUTE FOR FUSION STUDIES

DOE/ET-53088-413 IFSR #413

Thermonuclear Instability of Global-Type Shear Alfvén Modes

J.W. Van Dam
IFS-UT-Austin
Austin, Texas 78712
G.Y. Fu
École Polytechnique Fédérale de Lausanne
CH-1007 Lausanne, Switzerland
and
C.Z. Cheng
PPPL-Princeton University
Princeton, New Jersey 08543

January 1990

THE UNIVERSITY OF TEXAS

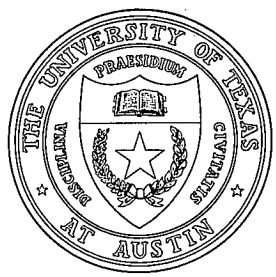

AUSTIN

Thermonuclear Instability of Global-Type Shear Alfvén Modes

J.W. Van Dam
Institute for Fusion Studies
The University of Texas at Austin
Austin, Texas 78712, U.S.A.

G.Y. Fu
Centre de Recherches en Physique des Plasmas
Association Euratom-Confédération Suisse
École Polytechnique Fédérale de Lausanne
21, Av. des Bains
CH-1007 Lausanne, Switzerland
and
C.Z. Cheng
Plasma Physics Laboratory
Princeton University
Princeton, New Jersey 08543, U.S.A.

Abstract

The effects of thermonuclear alpha particles on the stability of global-type shear Alfvén waves in toroidal geometry in an ignition tokamak experiment are described. The presence of finite toroidicity can lead to stabilization of the so-called global shear Alfvén eigenmode. However, toroidicity induces a new global shear Alfvén eigenmode, which can be strongly destabilized via transit resonance with alpha particles. In the proposed International Thermonuclear Experimental Reactor, due to its large size and low density, this latter mode is found to be benign.

1 Introduction

Ignition tokamak experiments, several of which are being proposed for the near future, such as the Compact Ignition Tokamak (CIT), the Fusion Ignition Experiment (IGNITEX), and the International Thermonuclear Experimental Reactor (ITER), will contain alpha particles produced by fusion reactions. These alpha particles will have very high energies and will not be in thermodynamic equilibrium. Consequently, it may be possible for "thermonuclear" drift-type instabilities to be excited in a burning plasma, with the alpha particle density inhomogeneity as the free energy source. Typically, the alpha particle pressure gradient scale length L_α compared to the plasma minor radius a is estimated as $L_\alpha/a = |a\, d(\ln n_\alpha)/dr|^{-1} \lesssim 0.4$ for ignition parameters.

In the work described here, we will focus our attention on the destabilization of shear Alfvén waves by alpha particles. For typical ignition parameters the alpha particle velocity $v_\alpha = (\varepsilon_\alpha/M_\alpha)^{1/2} = 9 \times 10^8\,\mathrm{cm/sec}$ for an energy of 3.5 MeV can be comparable in magnitude to the Alfvén speed $v_A = B/(N_i M_i)^{1/2}$. Thus, it is possible that the circulating alpha particles could destabilize shear Alfvén waves through inverse Landau damping at the $\omega \simeq k_{||} v_{||\alpha}$ wave-particle resonance, when ω is comparable to the shear Alfvén mode frequency $\omega_A = k_{||} v_A$. Here, $k_{||} = (m - nq)/qR$ is the parallel wavenumber for linearized waves that are Fourier decomposed as $\exp[i(m\theta - n\phi - \omega t)]$, with (n, m) and (ϕ, θ) the toroidal and poloidal mode numbers and the toroidal and poloidal angles, respectively. Also, $q(r)$ is the tokamak safety factor, and R is the major radius.

Various types of shear Alfvén waves can exist in a tokamak plasma. The ideal MHD equation of motion, written in cylindrical geometry, shows that the coefficient of the second order radial derivative term vanishes at those radial locations where the shear Alfvén resonance condition $\omega^2 = k_{||}^2 v_A^2$ holds. Frequencies ω that satisfy $\min[\omega_A^2(r)] \leq \omega^2 \leq \max[\omega_A^2(r)]$

then lie in the shear Alfvén continuum. This resonance leads to a singular mode structure; however, if electron parallel dynamics and ion finite Larmor radius effects are included, one obtains a nonsingular solution known as the kinetic Alfvén wave (KAW). Its mode structure is fairly localized, and hence it experiences strong electron Landau damping.

In addition, there are two global types of shear Alfvén waves, which have radially extended mode structure and low mode numbers n and m. The first type of global shear Alfvén wave is a regular, spatially nonresonant mode whose frequency lies just below the minimum of the continuum, i.e., $\omega < k_{||} v_A$ and $k_{||} \neq 0$. This mode is called the Global Alfvén Eigenmode (GAE). The other type of global shear Alfvén mode exists only in toroidal geometry and is called the Toroidicity-Induced Alfvén Eigenmode (TAE). Its frequency lies with "gaps" in the shear Alfvén continuum, which are created due to toroidal coupling.

The destabilization of shear Alfvén waves was first studied qualitatively by Mikhailovskii,[1] using a local dispersion relation. By including finite Larmor radius effects to discretize the continuum, Rosenbluth and Rutherford[2] found that the Kinetic Alfvén Wave can be destabilized by alpha particles. Tsang *et al.*[3] studied the details of the same problem numerically and reached a similar conclusion. Li *et al.*[4] found in cylindrical geometry that the Global Alfvén Eigenmode could be destabilized in a similar manner by transit wave-particle resonant interactions with super-Alfvénic alpha particles, although with weak growth rates. The existence of the Toroidicity-Induced Alfvén Eigenmode was shown in the ideal MHD limit, but without alpha particles.[5]

Our studies[6,7] show that the Global Alfvén Eigenmode tends to become completely stabilized in toroidal geometry, since finite toroidicity couples GAE modes with different poloidal mode numbers, thus enhancing the damping due to the sideband shear Alfvén Landau resonance. Moreover, electron damping due to the magnetic curvature drift is found to be further stabilizing for the GAE mode. However, we find[7–9] that the Toroidicity-Induced Alfvén Eigenmode, which is also destabilized by alpha particles through their transit (and

bounce) resonance, is a fairly strong instability, with kinetic effects modifying this unstable behavior only slightly. Therefore, this latter mode appears to be important for the confinement of alpha particles in an ignited tokamak device. However, for the specific parameters that are being proposed for the ITER device, we find that the $n = 1$ TAE mode is, in fact, stable.

Section 2 of this paper will discuss the GAE modes and how they are stabilized by finite toroidicity and electron damping. Section 3 will describe alpha particle excitation of the TAE global modes. Section 4 will present similar computational results for the TAE modes, obtained from a two-dimensional nonvariational numerical code. Section 5 considers the specific application of the theory for the TAE modes to the ITER tokamak. Concluding comments will be given in Section 6.

2 Stability of Global Alfvén Eigenmodes

In the cylindrical limit ($a/R \rightarrow 0$), the GAE mode has been found to be destabilized by inverse Landau resonance with transiting alpha particles.[4,10] The alpha particles are more appropriately modeled with a slowing-down distribution than with a Maxwellian, and at $L_\alpha/a \cong 0.4$ the growth rate is 10^{-3} of the mode frequency. Recall that the inverse Landau resonance in the alpha particle kinetic response is $\omega \cong k_\parallel^{(m\pm1)} v_{\parallel\alpha} \gg \mathbf{k}_\perp \cdot \mathbf{v}_{d\alpha}$, since the magnetic curvature drift velocity ($v_{d\alpha} \propto \cos\theta$) introduces coupling to the $m \pm 1$ sidebands, which then couple back to the main mode m.

When the effect of toroidal geometry is incorporated, however, we find the new result that finite toroidicity can stabilize the GAE modes via coupling to electron Landau damped sideband modes that resonate with the shear Alfvén continuum.[6,7] Shown in Fig. 1 are the shear Alfvén continua in cylindrical geometry for toroidal mode number $n = 1$ and poloidal mode numbers $m = -1, -2$, and -3. In particular, the eigenfrequency of the cylindrical GAE with mode $(n, m) = (1, -2)$ is located just below the minimum of the $m = -2$ continuum, as

indicated by the dotted line. In toroidal tokamak geometry, the cylindrical $(1,-2)$ mode will be coupled to sidebands, especially the $(1,-3)$ poloidal mode and the $(1,-1)$ mode, as well as other more distant poloidal modes. In particular, we observe that the sideband $(1,-1)$ mode has an Alfvén resonance near the edge of the plasma. We will find that this Alfvén resonance enhances the parallel electron Landau damping and has a stabilizing effect.

The theoretical description is contained in the following general wave equation:

$$\nabla \times \nabla \times \mathbf{E} - \frac{\omega^2}{c^2} \boldsymbol{\chi}_f \cdot \mathbf{E} = \frac{\omega^2}{c^2} (\boldsymbol{\chi}_k + \boldsymbol{\chi}_\alpha) \cdot \mathbf{E} \,, \tag{1}$$

where the terms on the left-hand side correspond to the ideal MHD dynamics, and the terms on the right-hand side represent the kinetic effects of both the bulk plasma and the alpha particles. Here, $\mathbf{E}$ is the perturbed electric field, and the susceptibility tensor $\boldsymbol{\chi}$ has been separated into three parts: $\boldsymbol{\chi}_f = (c/v_A)^2(\mathbf{I} - \widehat{bb})$ for the plasma fluid response; $\boldsymbol{\chi}_k$ for the core plasma kinetic response (including ion FLR and parallel electron dynamics, but in the low frequency limit $\omega/\omega_{ci} < 1$); and $\boldsymbol{\chi}_\alpha$ for the drift-kinetic alpha particle response. In toroidal geometry, all the terms in Eq. (1) contain some mode coupling. Here we keep only the coupling from the left-hand side of Eq. (1) and neglect the toroidicity effects contained in the kinetic response from the cold component and alpha particles. This approximation may be justified for the following reasons. The mode coupling from the alpha particles is small because of the ordering $\beta_\alpha \ll 1$. Also, the kinetic term $\boldsymbol{\chi}_k$ is small except near the shear-Alfvén resonance, so we can neglect the toroidicity contribution from $\boldsymbol{\chi}_k$, at least away from the Alfvén resonance. Furthermore, we find that near the resonance the kinetic mode coupling can also be neglected, since the $\mathcal{O}(\varepsilon)$ mode coupling contributions due to the ω^2/v_A^2 and $k_\parallel^2$ terms combine and therefore are larger than the corresponding kinetic mode coupling contribution. Hence, we may use the cylindrical form of $\boldsymbol{\chi}_k$ in Eq. (1).

To simplify the mode coupling due to the operator term $\nabla \times \nabla \times$ and the $\boldsymbol{\chi}_f$ term, we assume concentric circular flux surfaces and use the following toroidal coordinates: $x =$

$R\cos(-\varphi)$, $y = R\sin(-\varphi)$, $z = r\sin\theta$, $R = R_0 + r\cos\theta$. In terms of this toroidal coordinate system and with the representation $\mathbf{E} = (E_r, E_\perp, E_\parallel)$ for the electric field, we find the components of $\nabla \times \nabla \times \mathbf{E}$ to be

$$(\nabla \times \nabla \times \mathbf{E})_r = \left(\frac{1}{R^2}\frac{\partial^2}{\partial\varphi^2} + \frac{1}{r^2 R}\frac{\partial}{\partial\theta}R\frac{\partial}{\partial\theta}\right) E_r +$$

$$\left(-\frac{1}{r^2 R}\frac{\partial}{\partial\theta}R\frac{\partial}{\partial r}\frac{r}{\sqrt{1+\delta^2}} + \frac{1}{R^2}\frac{\partial}{\partial\varphi}\frac{\partial}{\partial r}\frac{R\delta}{\sqrt{1+\delta^2}}\right) E_\perp -$$

$$\left(\frac{1}{rR}\frac{\partial}{\partial\theta}R\frac{\partial}{\partial r}\frac{r\delta}{\sqrt{1+\delta^2}} + \frac{1}{R^2}\frac{\partial}{\partial\varphi}\frac{\partial}{\partial r}\frac{R}{\sqrt{1+\delta^2}}\right) E_\parallel \,, \tag{2}$$

$$(\nabla \times \nabla \times \mathbf{E})_\perp = \left(-\frac{1}{R\sqrt{1+\delta^2}}\frac{\partial}{\partial r}\frac{R}{r}\frac{\partial}{\partial\theta} + \frac{\delta}{r\sqrt{1+\delta^2}}\frac{\partial}{\partial r}\frac{r}{R}\frac{\partial}{\partial\varphi}\right) E_r +$$

$$\left[\frac{1}{R\sqrt{1+\delta^2}}\left(\frac{\partial}{\partial\varphi}+\frac{1}{q}\frac{\partial}{\partial\theta}\right)\frac{1}{R}\left(\frac{\partial}{\partial\varphi}+\frac{1}{q}\frac{\partial}{\partial\theta}\right)\frac{1}{\sqrt{1+\delta^2}}+\right.$$

$$\left.\frac{1}{R\sqrt{1+\delta^2}}\frac{\partial}{\partial r}\frac{R}{r}\frac{\partial}{\partial r}\frac{r}{\sqrt{1+\delta^2}} + \frac{\delta}{r\sqrt{1+\delta^2}}\frac{\partial}{\partial r}\frac{r}{R}\frac{\partial}{\partial r}\frac{R\delta}{\sqrt{1+\delta^2}}\right] E_\perp +$$

$$\left[\frac{1}{R\sqrt{1+\delta^2}}\left(\frac{\partial}{\partial\varphi}+\frac{1}{q}\frac{\partial}{\partial\theta}\right)\frac{1}{rR}\left(\delta^2 q\frac{\partial}{\partial\varphi}-\frac{\partial}{\partial\theta}\right)\frac{R}{\sqrt{1+\delta^2}}+\right.$$

$$\left.\frac{1}{R\sqrt{1+\delta^2}}\frac{\partial}{\partial r}\frac{R}{r}\frac{\partial}{\partial r}\frac{r\delta}{\sqrt{1+\delta^2}} - \frac{\delta}{r\sqrt{1+\delta^2}}\frac{\partial}{\partial r}\frac{r}{R}\frac{\partial}{\partial r}\frac{R}{\sqrt{1+\delta^2}}\right] E_\parallel \,, \tag{3}$$

with $\delta = r/qR$. It is straightforward to show that the infinite aspect ratio limit of Eqs. (2) and (3), i.e., with R replaced by R_0, reduces to exactly the same equations as were derived by Ross *et al.*[11] for cyindrical geometry. Following Ref. 11, we shall not make use of the parallel component of Ampere's law; instead, as before, $E_\parallel$ can be eliminated in terms of E_r and $E_\perp$ by means of $\nabla \cdot \mathbf{J} = 0$:

$$E_\parallel = -\frac{B}{\chi_{\parallel,\parallel}}\left(R^2\mathbf{B}\cdot\nabla\right)^{-1}\left(R^2\nabla\cdot(\boldsymbol{\chi}\cdot\mathbf{E})_\perp\right) \,. \tag{4}$$

Notice that the operator $R^2\mathbf{B}\cdot\nabla = R_0B_0(\partial/\partial\varphi + \partial/q\partial\varphi)$ contains no toroidicity, and hence we can invert it algebraically. In any case, we will neglect the toroidicity due to $E_{||}$ terms since these are kinetic terms.

Next, Eq. (1) can be expanded straightforwardly, with the inverse aspect ratio $\varepsilon = a/R$ as a small parameter:

$$\tilde{L} = \tilde{L}_0 + \varepsilon\frac{r}{a}(2\cos\theta\tilde{L}_S + 2i\sin\theta\tilde{L}_A)\ . \tag{5}$$

Here $\tilde{L}_0$ is the cylindrical matrix operator whose components are given by

$$L_{rr} = \frac{\omega^2}{v_A^2} - k_{||}^2 - k_\perp^2 - \frac{11}{8}b_i\,k_\perp^2 + \frac{d}{dr}\frac{3}{8}b_i\frac{1}{r}\frac{d}{dr}r$$
$$+ k_{||}\frac{d}{dr}k_{||}^{-1}d_e\frac{v_A^2}{\omega^2}\frac{1}{r}\frac{d}{dr}r\frac{\omega^2}{v_A^2} + S_{rr} - Q_{m-1} - Q_{m+1}\ , \tag{6}$$

$$L_{r\perp} = i\left[-\frac{k_\perp}{r}\frac{d}{dr}r - \frac{k_\perp}{r}\frac{11}{8}b_i\frac{d}{dr}r + \frac{d}{dr}\frac{3}{8}b_i\,k_\perp\right.$$
$$\left. + k_{||}\frac{d}{dr}k_{||}^{-1}d_e\,k_\perp - iS_{r\perp} + Q_{m-1} - Q_{m+1}\right]\ , \tag{7}$$

$$L_{\perp\perp} = \frac{\omega^2}{v_A^2} - k_{||}^2 + \frac{d}{dr}\frac{1}{r}\frac{d}{dr}r + \frac{d}{dr}\frac{11}{8}b_i\frac{1}{r}\frac{d}{dr}r - \frac{3}{8}b_i\,k_\perp^2$$
$$- d_e\,k_\perp^2 + S_{\perp\perp} - Q_{m-1} - Q_{m+1}\ , \tag{8}$$

$$L_{\perp r} = -i\left[-\frac{d}{dr}k_\perp - \frac{d}{dr}\frac{11}{8}b_i\,k_\perp + k_\perp\frac{3}{8}b_i\frac{1}{r}\frac{d}{dr}r\right.$$
$$\left. + k_\perp d_e\frac{v_A^2}{\omega^2}\frac{1}{r}\frac{d}{dr}r\frac{\omega^2}{v_A^2} - iS_{\perp r} - Q_{m-1} + Q_{m+1}\right]\ . \tag{9}$$

Here $b_i = (\omega^2/v_A^2)\rho_i^2$ and $d_e = (k_{||}\rho_s)^2\left[1 + (\omega/k_{||}v_e)Z(\omega/k_{||}v_e)\right]^{-1}$, with $\rho_i^2 = 2T_i/m_i\omega_{ci}^2$ the ion Larmor radius, $\rho_s^2 = T_e/m_i\omega_{ci}^2$, ω_{ci} the ion cyclotron frequency, ω the frequency of the perturbed field, and v_e the electron thermal velocity. The wave numbers are given approximately by $k_\perp = m/r$ and $k_{||} = (n - m/q)/R$, where n and m are the toroidal mode

number and the poloidal mode number, respectively, and R is the major radius. The terms S_{rr}, $S_{r\perp}$, $S_{\perp\perp}$, and $S_{\perp r}$, which arise from the equilibrium current and the shear of the magnetic field, are given in Ref. 11, and the term $Q_{m\pm1}$ is the alpha particle contribution given in Ref. 4 as follows:

$$Q_{m\pm1} = -i\,\frac{\beta_\alpha}{2R^2}\left(P_{m\pm1} - \frac{\omega_{*\alpha m}}{\omega}\,R_{m\pm1}\right)\,, \tag{10}$$

$$P_{m\pm1} = \frac{\pi\omega}{v_\alpha^4}\int d^3v\left(v_\perp^2/2 + v_\parallel^2\right)^2\left(-T_\alpha\frac{\partial f_{\alpha0}}{\partial E}\right)\delta(\omega - k_\parallel v_\parallel)\,, \tag{11}$$

$$R_{m\pm1} = \frac{\pi\omega}{v_\alpha^4}\int d^3v\left(v_\perp^2/2 + v_\parallel^2\right)^2 f_{\alpha0}\delta(\omega - k_\parallel v_\parallel)\,. \tag{12}$$

Here, $\beta_\alpha = 8\pi n_\alpha T_\alpha/B^2$ and $v_\alpha^2 = 2T_\alpha/m_\alpha$, with T_α, n_α, β_α, and v_α being the temperature, density, beta value, and thermal velocity of the alpha particles, respectively. Also, $f_{\alpha0}$ is the alpha particle equilibrium distribution function.

The toroidal terms $\tilde{L}_S$ and $\tilde{L}_A$ are given by

$$(\tilde{L}_S)_{rr} = -\frac{1}{R_0^2}\frac{\partial^2}{\partial\varphi^2}\,, \tag{13}$$

$$(\tilde{L}_S)_{r\perp} = -\frac{1}{2r^3}\frac{\partial}{\partial\theta}\frac{\partial}{\partial r}r^2\delta_0^2 - \frac{1}{R_0}\frac{\partial}{\partial\varphi}\frac{\partial}{\partial r}\frac{\delta_0}{\sqrt{1+\delta_0^2}}\,, \tag{14}$$

$$(\tilde{L}_S)_{\perp r} = -\frac{1}{2}\left(\frac{1}{\sqrt{1+\delta_0^2}} - \delta_0^2 + \frac{\delta_0^2}{r}\frac{\partial}{\partial r}\right)\frac{\partial}{\partial\theta} - \frac{\delta_0}{rR_0\sqrt{1+\delta_0^2}}\left(\frac{3}{2} + r\frac{\partial}{\partial r}\right)\frac{\partial}{\partial\varphi}\,, \tag{15}$$

$$(\tilde{L}_S)_{\perp\perp} = \frac{1}{2}\left[\delta_0^2\frac{\partial}{\partial r}\frac{1}{r}\frac{\partial}{\partial r}\frac{r}{\sqrt{1+\delta_0^2}} + \frac{1}{r\sqrt{1+\delta_0^2}}\frac{\partial}{\partial r}\frac{1}{r}\frac{\partial}{\partial r}r^2\delta_0^2\right.$$

$$\left. + \frac{1}{r^2\sqrt{1+\delta_0^2}}\frac{\partial}{\partial r}\frac{r}{\sqrt{1+\delta_0^2}} - \frac{\delta_0}{r\sqrt{1+\delta_0^2}}\frac{\partial}{\partial r}\frac{\delta_0}{\sqrt{1+\delta_0^2}}\right.$$

$$- \frac{2\delta_0}{r\sqrt{1+\delta_0^2}} \frac{\partial}{\partial r} r \frac{\partial}{\partial r} \frac{\delta_0}{\sqrt{1+\delta_0^2}} \Bigg] - \frac{1}{R_0^2} \left(\frac{\partial}{\partial \varphi} + \frac{1}{q} \frac{\partial}{\partial \theta} \right)^2 , \tag{16}$$

$$(\tilde{L}_A)_{rr} = \frac{i}{2r^2} \frac{\partial}{\partial \theta} , \tag{17}$$

$$(\tilde{L}_A)_{r\perp} = -2i \left(\frac{1}{r^2} \frac{\partial}{\partial r} \frac{r}{\sqrt{1+\delta_0^2}} + \frac{1}{r^3} \frac{\partial}{\partial r} r^2 \delta_0^2 \right) , \tag{18}$$

$$(\tilde{L}_A)_{\perp r} = 0 , \tag{19}$$

$$(\tilde{L}_A)_{\perp\perp} = -\frac{i\delta_0}{4rR_0\sqrt{1+\delta_0^2}} \left(\frac{\partial}{\partial \varphi} + \frac{1}{q} \frac{\partial}{\partial \theta} \right) . \tag{20}$$

Under Fourier transformation and keeping only nearest-neighbor sideband coupling, we find that Eq. (1) then becomes an infinite set of coupled equations:

$$\hat{\varepsilon}(\tilde{L}_S + \tilde{L}_A)_{m-1} \tilde{E}_{m-1} + (\tilde{L}_0)_m \tilde{E}_m + \hat{\varepsilon}(\tilde{L}_S - \tilde{L}_A)_{m+1} \tilde{E}_{m+1} = 0 , \tag{21}$$

where $\hat{\varepsilon} = \varepsilon r/a$ and $\tilde{E} = \begin{pmatrix} E_r \\ E_\perp \end{pmatrix}$. In the limit of $\varepsilon \to 0$, Eq. (21) reduces to the cylindrical form, i.e., $\tilde{L}_{0m}\tilde{E}_m = 0$. For nonzero ε, we have an infinite series of coupled equations. To truncate this infinite series, we consider only three poloidal modes. This is consistent with expanding only to first order in ε. Thus, we finally obtain the following six-by-six matrix of coupled second-order differential equations to be solved numerically:

$$\begin{pmatrix} (\tilde{L}_0)_{m-1} & \hat{\varepsilon}(\tilde{L}_S - \tilde{L}_A)_m & 0 \\ \hat{\varepsilon}(\tilde{L}_S + \tilde{L}_A)_{m-1} & (\tilde{L}_0)_m & \hat{\varepsilon}(\tilde{L}_S - \tilde{L}_A)_{m+1} \\ 0 & \hat{\varepsilon}(\tilde{L}_S + \tilde{L}_A)_m & (\tilde{L}_0)_{m+1} \end{pmatrix} \begin{pmatrix} \tilde{E}_{m-1} \\ \tilde{E}_m \\ \tilde{E}_{m+1} \end{pmatrix} = 0 . \tag{22}$$

We consider the numerical solution of Eq. (22) for the $(1, -2)$ mode as a typical GAE mode with $n \neq 0$, for CIT-like parameters: $R = 1.4\,\mathrm{m}$, $a = 0.67\,\mathrm{m}$, $B_0 = 10\,\mathrm{T}$, $n_e(0) = 10^{21}\,\mathrm{m}^{-3}$, $n_\alpha(0) = 2 \times 10^{19}\,\mathrm{m}^{-3}$, and $T_{e_0} = 30\,\mathrm{keV} = T_{i_0}$. The profiles were taken to be:

$n = n_0\,[1 - r^2/(a+d)^2]$, $T_{e,i} = T_{0e,i}\,[1 - (r/a)^2]$, and $q = 1 + 2(r/a)^2$, where the value of d is chosen such that the plasma density at the edge is 10% of its central value: $n(a)/n(0) = 0.1$. The alpha particle density profile is taken to be $n_\alpha(r) = n_\alpha(0)\exp(-r^2/L_\alpha^2)$, where L_α is the alpha particle density gradient scale length. Notice that the value of the edge density is not zero, in order to have the Alfvén frequency be finite at the edge. Also we choose the edge density value to be small enough for a sideband resonance to exist. For the sake of comparison and of numerical calculation, we use ε as an independent variable in Eq. (22). Thus, for $\varepsilon = 0$, our calculation will recover the cylindrical eigenvalues. The known cylindrical eigenvalues will then provide us with very good guesses for the corresponding toroidal eigenvalues, which can be traced as the value of ε is increased.

Shown in Fig. 2 is the radial electric field for the main poloidal mode $(1, -2)$ and its two sidebands $(1, -1)$ and $(1, -3)$, for $\varepsilon = 0.1$. Figure 3 shows the sideband $(1, -1)$ for various values of the toroidicity parameter ε. Figure 4 shows both the Landau damping rate obtained without alpha particles, as well as the growth rate induced by alpha particles, with $L_\alpha/a = 0.25$. This value for the alpha particle density scale length L_α corresponds to the maximum growth rate in the cylindrical limit. The real frequency of the mode is $\omega_r = 7.95 \times 10^6\,\mathrm{s}^{-1}$.

We find that the structure of the sideband $(1, -1)$ near its Alfvén resonance has two distinctive types of behavior depending on the value of ε. For small values (viz., $\varepsilon < 0.3$), the sideband $(1, -1)$ is like an Airy function and the mode propagates toward the center of the plasma. In fact, Stix[12] has shown that for $\beta_e/(m_e/m_i) > 1$ at the resonance, the essential evanescent compressional wave at the edge of the plasma will convert to a kinetic Alfvén wave, which propagates toward the high density region. Our results confirm this physical process. Furthermore, as ε increases, we observe that the sideband resonance shifts toward the edge of the plasma. As a result, the value of $\beta_e/(m_e/m_i)$ at the resonance decreases and eventually becomes less than unity, at which point the KAW becomes the so-called

cold surface Alfvén wave.[11,12] Notice that the toroidal coupling will lower the $(1,-1)$ Alfvén continuum, and therefore its resonance moves toward the outside as ε increases. Finally, for $\varepsilon = 0.48$, which corresponds to our ignition parameters, the $(1,-1)$ singularity simply disappears.

More or less related to these observations, we also find that there are three distinct stages for the Landau damping rate γ_L and the total growth rate γ including the alpha particles. For small values of $\varepsilon < 0.1$, we find the scalings $\gamma_L \propto \varepsilon^2$ and $\gamma \propto \varepsilon^2$; for intermediate values of ε, $0.1 < \varepsilon < 0.2$, we find that both scale linearly, $\gamma_L \propto \varepsilon$ and $\gamma \propto \varepsilon$; for still larger values, $\varepsilon > 0.25$, γ_L eventually saturates and begins to decrease, while the trend for γ is exactly the opposite.

Recall that the electron Landau damping rate for the localized KAW mode is much higher than that for the GAE modes. Thus the toroidal GAE mode, which is a mixture of the cylindrical GAE mode and a sideband KAW mode, has a greater damping rate. On the other hand, the KAW sideband should contribute little to the alpha particle destabilization since it is localized near the edge of the plasma where few alpha particles reside. Therefore, as ε increases, the electron Landau damping is enhanced and the total growth rate decreases. For $\varepsilon = 0.1$, the mode is stabilized. However, as the value of ε is raised further, the Landau damping begins to saturate and, eventually, to decrease; consequently, the stabilization through toroidal coupling is weakened. The reason for the reduction in the Landau damping is the shifting of the $(1,-1)$ resonance toward the edge of the plasma as ε increases; correspondingly, the coupling between the GAE mode and the KAW sideband is reduced. For the ignition value of $\varepsilon = 0.48$, the GAE mode is still stabilized. Moreover, the inclusion of the additional sideband $(1,0)$ is expected to shift the $(1,-1)$ resonance toward the center of the plasma, as opposed to the $(1,-2)$ mode. Thus we expect the stabilizing effect to be further enhanced.

We are able to reproduce the scaling of the frequency shift and the sideband amplitude

due to finite toroidicity if we make an analogy with quantum mechanical perturbation theory. Equation (22) can be viewed as an eigenvalue equation, with the diagonal elements as the unperturbed operators and the off-diagonal elements as the perturbation. In the limit of $\varepsilon \to 0$ or zero perturbation, the eigenvalue of our system reduces to the unperturbed spectrum or the cylindrical spectrum. For small ε, the unperturbed spectrum is non-degenerate; consequently the amplitude of the perturbed sideband is proportional to ε and the frequency shift $\delta\omega$ has the scaling $\delta\omega \propto \varepsilon^2$. As ε is increased, the spectrum becomes degenerate and we must invoke the method of degenerate perturbation theory. In this case, we have the linear scaling $\delta\omega \propto \varepsilon$. These analytical scalings agree well with our numerical results for $\varepsilon < 0.2$.

The GAE modes with $n = 0$ cannot be treated with this theory, because two sidebands are no longer adequate to describe the toroidal coupling. These modes have been investigated with another numerical code, and the results will be described in Section 4.

Finally, we examine the effect of electron damping due to the curvature drift. This damping occurs even when toroidicity is not included, and so for the sake of simplicity we examine this effect in cylindrical geometry ($a/R \to 0$). Previous work[2-4,10] only considered the contribution of the fusion alpha particles to the perturbed current that is due to the alpha particle magnetic curvature drift, which is destabilizing through the inverse Landau damping process. Similar terms for the electrons and ions were ignored since their drift velocities are much smaller than that of the alpha particles and their thermal velocities are very different from the Alfvén phase velocity. Nonetheless, we find that for GAE modes the electron contribution to the drift current term can indeed be comparable in magnitude to the alpha particle contribution. The reason is simply that the electron density is much higher than that of the alpha particles, especially away from the plasma center, although the electron temperature is much lower than the alpha particle temperature and the electron thermal velocity is much larger than the Alfvén phase velocity. Notice that this electron curvature drift term is always stabilizing since $\omega_{*e}/\omega_A \ll 1$, where ω_{*e} is the electron

diamagnetic drift frequency. The ion contribution can still be neglected, since its thermal velocity is much smaller than the Alfvén phase velocity. Shown in Fig. 5 for typical ignition parameters is the growth rate of the GAE $(0,-2)$ mode (solid line) with the effect of the electron curvature drift term included; for comparison, the growth rate without the electron drift term (dashed line) is also shown. We observe that for these parameters the electron drift term overcomes the alpha particle term and stabilizes the GAE mode.

To gain a quantitative understanding of the electron drift effect, we consider the local dispersion relation, including both the alpha particle and electron magnetic drift terms:

$$\gamma/\omega_A = \frac{\beta_\alpha}{2k_\parallel^2 R^2}\left(\frac{\omega_{*\alpha}}{\omega}-\frac{1}{2}\right)\frac{v_A}{v_\alpha}F\left(\frac{2v_A}{v_\alpha}\right)$$

$$-\frac{\beta_e}{2k_\parallel^2 R^2}\frac{v_A}{v_e}-\left(k_r^2+k_\perp^2\right)\rho_s^2\pi^{1/2}\frac{v_A}{v_e}\,, \qquad (23)$$

where $F(u)=(1+2u^2+4u^4)\exp(-u^2)$. The first term represents the effect of the alpha particles (modeled with a slowing-down distribution) and is destabilizing if $\omega_{*\alpha}>\omega$. The second term on the right-hand side of Eq. (23) arises from the electron curvature drift, and the third term is the usual electron Landau damping due to parallel electron motion. Note that the Landau damping is proportional to $(k_r^2+k_\perp^2)\rho_s^2$, so that for a global mode like GAE mode, the damping is very weak, whereas for the radially localized KAW modes with their large k_r, Landau damping can be quite large. Also note that the third term is smaller by a factor of $\omega_{CA}^2/\omega_{ci}^2 \ll 1$ compared to the second term, where ω_{CA} is the compressional Alfvén frequency. Thus we can estimate the overall electron damping rate as

$$\gamma_e/\omega_A \approx -\frac{\beta_e}{2k_\parallel^2 R^2}\frac{v_A}{v_e} = -1.0\times 10^{-3} \qquad (24)$$

for the GAE $(0,-2)$ mode with ignition parameters. Numerically we obtain $\gamma_e/\omega_A = -1.7\times 10^{-3}$ and a maximum alpha particle-induced growth rate of $\gamma_\alpha/\omega_A = 1.3\times 10^{-3}$ at $L_\alpha/a = 0.45$. Therefore the GAE $(0,-2)$ mode is stabilized by the electron damping due to their magnetic curvature drift, even without the stabilizing effect of finite toroidicity.

3 Stability of Toroidicity-Induced Alfvén Eigenmodes

The TAE mode is a shear Alfvén wave that can exist only in toroidal geometry. For example, if the cylindrical geometry Alfvén continua corresponding to modes with toroidal and poloidal mode numbers (n, m) and $(n, m+1)$ intersect at $r = r_0$, where $q(r_0) = (m+1/2)/n$, then toroidicity resolves this degeneracy with a "gap" in the coupled toroidal continuum. Frequencies within this gap are forbidden (analogous to Brillouin zones for the motion of electrons in a periodic lattice potential), except for a certain discrete frequency, which constitutes the TAE mode. In as much as this is a global mode (i.e., low mode number and radially non-localized), its stability can be a significant issue.

Cheng *et al.* were the first to show the existence of both low-mode-number[5] and high-mode-number[13] TAE modes. Those theories were developed in the MHD limit, without alpha particles. Here, we describe how the presence of highly energetic alpha particles, as in an ignited tokamak plasma, can strongly excite the TAE mode.[8] This result is relevant to plasma confinement in proposed ignition experiments.

The theory to describe this physics becomes analytically tractable by adopting a low beta, large aspect ratio, circular flux surface tokamak equilibrium. Following Rosenbluth and Rutherford,[2] we describe the dynamics of the shear Alfvén wave with alpha particles by the linearized drift kinetic equation, using ϕ_1 the electrostatic potential and $A_{\|1}$ the parallel vector potential to represent the perturbed electromagnetic fields (this implies that $B_{\|1} = 0$ where $B_{\|}$ is the parallel magnetic field). We integrate the linearized drift kinetic equation over all velocities, multiply it by the charge e_s, and sum over all species (indexed by "s"), thus obtaining a moment equation for the perturbed current density:

$$\mathbf{b} \cdot \nabla j_{\|1} + \mathbf{b}_1 \cdot \nabla j_{\|} + \sum_s e_s \int d^3v \mathbf{v}_{ds} \cdot \nabla f_{1s} = -\nabla \cdot \left[\frac{i\omega c^2}{4\pi v_A^2} \nabla_\perp \phi_1 \right] \tag{25}$$

where the subscript "1" denotes perturbed quantities, $\mathbf{b}$ is the unit vector along the magnetic field, $j_{\|}$ is the plasma parallel current, e_s is the particle charge, f_{1s} is the perturbed

distribution function, B is the magnetic field strength, $v_A = B/(4\pi n_i m_i)^{1/2}$ is the Alfvén speed, and $\mathbf{v}_{ds} = [m_s c(\mu B + v_\parallel^2)/(e_s B^2)]\mathbf{b} \times \nabla B$ is the magnetic curvature drift velocity (in the low beta limit) with $\mu = v_\perp^2/2B$ the magnetic moment. The alpha particle contribution to the polarization current has been neglected, owing to the orderings $n_\alpha \ll n_i$ and $\beta_\alpha \ll \beta_i$. However, the perturbed alpha current caused by the drift velocity $\mathbf{v}_{d\alpha}$ due to the gradient and curvature of the equilibrium magnetic field is retained, because of the very high energy of the alpha particles. The perturbed electron drift current will also be retained, whereas that of the plasma ions may be neglected because $v_i \ll v_A$ where $v_i = (2T_i/m_i)^{1/2}$ is the ion thermal speed. With the help of Ampére's law and using the quasi-neutrality condition to eliminate $A_{\parallel 1}$ in term of ϕ_1, one can rewrite Eq. (25) as follows:

$$\mathbf{b}\cdot\nabla\nabla_\perp^2\mathbf{b}\cdot\nabla\phi_1 - \frac{\mathbf{b}\times\nabla(\mathbf{b}\cdot\nabla\phi_1)}{B}\cdot\nabla\left(\frac{4\pi}{c}j_\parallel\right) + \nabla\cdot\frac{\omega^2}{v_A^2}\nabla_\perp\phi_1$$

$$= \sum_s \frac{i4\pi\omega}{c^2}e_s\int d^3v\mathbf{v}_{ds}\cdot\nabla f_{1s} \tag{26}$$

For simplicity, we assume concentric magnetic flux surfaces. Expanding the toroidicity effect to first order in the inverse aspect ratio $a/R < 1$ and retaining only the two dominant poloidal modes for the TAE mode, we then arrive at the following two coupled second-order eigenmode equations for the poloidal electrical field $E \propto \phi_1/r$:

$$\left[\frac{d}{dr}r^3\left(\frac{\omega^2}{v_A^2} - k_{\parallel m}^2 + \sum_s A_{s,m}\right)\frac{d}{dr} - (m^2-1)r\left(\frac{\omega^2}{v_A^2} - k_{\parallel m}^2 + \sum_s A_{s,m}\right)\right.$$

$$\left. + \left(\frac{\omega^2}{v_A^2}\right)' r^2 + \sum_s mB'_{s,m}r^2\right]E_m + \left[\varepsilon\frac{d}{dr}\frac{\omega^2}{v_A^2}\frac{r^4}{a}\frac{d}{dr}\right]E_{m+1} = 0 \tag{27}$$

$$\left[\frac{d}{dr}r^3\left(\frac{\omega^2}{v_A^2} - k_{\parallel m+1}^2 + \sum_s A_{s,m+1}\right)\frac{d}{dr} - \Big((m+1)^2-1\Big)r\left(\frac{\omega^2}{v_A^2} - k_{\parallel m+1}^2 + \sum_s A_{s,m+1}\right)\right.$$

$$\left. + \left(\frac{\omega^2}{v_A^2}\right)' r^2 + \sum_s (m+1)B'_{s,m+1}r^2\right]E_{m+1} + \left[\varepsilon\frac{d}{dr}\frac{\omega^2}{v_A^2}\frac{r^4}{a}\frac{d}{dr}\right]E_m = 0 \tag{28}$$

where $\varepsilon = 3a/2R$, the prime denotes radial differentiation, and the subscripts m and $m+1$ are the two dominant poloidal mode number. Also, $k_{\|m} = (n - m/q)/R$ is the parallel wavenumber, with R the major radius and q the safety factor. The quantities $A_{s,m} = Q_{s,m-1} + Q_{s,m+1}$ and $B_{s,m} = Q_{s,m-1} - Q_{s,m+1}$ represent the kinetic response arising from the curvature drift of species s with poloidal mode number m, with the quantities $Q_{s,m\pm1}$ defined in Eqs. (10)–(12). The forms for $A_{s,m}$ and $B_{s,m}$ can be derived by solving the linearized drift kinetic equation.[4] These two quantities originate from the drift current due to the perturbed electrical field with toroidal and poloidal mode number (n,m), when only the resonant part of the response is retained. The two contributions to $A_{s,m}$ and $B_{s,m}$, from the sideband resonances $\omega = k_{\|m\pm1}v_\|$, result from the poloidal variation of the particle drift velocity. Because of this, the resonant part of the perturbed particle distribution has poloidal variation $\exp[i(m \pm 1)\theta]$ in response to the perturbed field $E_m \exp(im\theta)$, although the perturbed drift current has the poloidal variation $\exp(im\theta)$, at least to lowest order in the inverse aspect ratio. Finally, we remark that the mode coupling due to this drift current is small by the ordering $\beta_s \ll 1$.

First, let us consider the MHD limit of Eqs. (27) and (28), dropping the kinetic terms A_s and B_s temporarily. In cylindrical geometry ($\varepsilon = 0$), the two poloidal modes E_m and E_{m+1} are decoupled. Then Eqs. (27) and (28) are singular at $\omega_1^2 = k_{\|m}^2 v_A^2$ and $\omega_2^2 = k_{\|m+1}^2 v_A^2$, respectively, which give the two cylindrical shear Alfvén continua. In tokamak geometry, Eqs. (27) and (28) are coupled due to the finite toroidicity, and the poloidal mode numbers are no longer good "quantum" numbers. The toroidal shear Alfvén continuum can be obtained by setting the determinant of the coefficients of the second-order derivative terms equal to zero, which yields the following two branches:

$$\omega_\pm^2 = \frac{k_{\|m}^2 v_A^2 + k_{\|m+1}^2 v_A^2 \pm \sqrt{\left(k_{\|m}^2 v_A^2 - k_{\|m+1}^2 v_A^2\right)^2 + 4\varepsilon^2 x^2 k_{\|m}^2 v_A^2 k_{\|m+1}^2 v_A^2}}{2(1-\varepsilon^2 x^2)} \tag{29}$$

where $x = r/a$ is the normalized radius. In particular, at the crossing point of the two

cylindrical continua where $k_{\|m} = -k_{\|m+1}$, or $q = (2m+1)/2n$, a gap appears whose width is given by

$$\Delta\omega = \omega_+ - \omega_- \cong 2\varepsilon x \left(\left|k_{\|m} v_A\right|\right)_{q-(2m+1)/2n} .$$

Figure 6 shows the toroidal continuum (solid curves) given by Eq. (29) for $n = -1, m = -2$, and $\varepsilon = 0.375$ with a constant density profile and $q(r) = 1 + (r/a)^2$; the cylindrical continua (dashed curves) are also shown in Fig. 6. The corresponding TAE mode structure is shown in Fig. 7; its eigenfrequency $\omega = 0.93 \left(\left|k_{\|m} v_A\right|\right)_{q=1.5}$ lies inside the continuum gap. The eigenmode was obtained by numerically solving Eqs. (27) and (28) with the shooting method. Note that the mode is peaked at the location of the gap, i.e., near the crossover point of the cylindrical continua.

Next we consider the kinetic effects of alpha particles and electrons on the TAE modes. The resonant contributions of these fast particles can be included perturbatively by assuming that the imaginary part of the frequency is small compared to the real part. To begin with, we expand the solution of Eqs. (27) and (28) as $E_m = E_{0,m} + \delta E_m$ and $\omega = \omega_0 + \delta\omega$, where $E_{0,m}$ and ω_0 are the MHD eigenfunction and eigenfrequency, respectively. We expand the coupled equations to first order in β_s (assuming $\beta_s < \varepsilon$). Exploiting the self-adjointness of the coupled equations, we obtain the change in frequency due to the kinetic terms as follows:

$$\frac{\delta\omega}{\omega_0} = -\frac{v_{A_0}^2}{2\omega_0^2}$$

$$\times \frac{\sum_{m,s}\left\langle r^3 E_{0,m}'^2 A_{s,m} + \left[(m^2-1)rA_{s,m} - r^2 A_{s,m}' - mr^2 B_{s,m}'\right] E_{0,m}^2\right\rangle}{\left\langle \sum_m \left[(r^3/\tilde{v}_A^2)\, E_{0,m}'^2 + (m^2-1)\,(r/\tilde{v}_A^2)\, E_{0,m}'^2 - (1/\tilde{v}_A^2)' r^2 E_{0,m}^2\right] + 2q\varepsilon\,(r^4/a\tilde{v}_A^2)\, E_{0,m}' E_{0,m+1}'\right\rangle} \tag{30}$$

where $\tilde{v}_A$ is the Alfvén velocity normalized to its value at the center of the plasma. Using Eq. (30), we calculate the growth rate for the TAE mode of Fig. 7. Figure 8 shows the growth rate (normalized to the real frequency) as a function of the alpha particle density scale length L_α, for the typical ignition tokamak parameters of $a/R = 1/4$, $\rho_{\alpha 0}/a = 0.05$, $v_{\alpha 0} = 2v_A$, $\beta_e(0) = 6\%$, and $\beta_\alpha(0) = 3\%$, for the profiles $\beta_\alpha = \beta_\alpha(0)\exp(-r^2/L_\alpha^2)$ and $\beta_e = \beta_e(0)(1-r^2/a^2)^3$. A maximum growth rate of $(\gamma/\omega_0)_{\max} = 2.5\times 10^{-2}$ is obtained at $L_\alpha = 0.5a$. For $L_\alpha < 0.87a$, the TAE mode is unstable.

In the limit of large aspect ratio, the TAE mode is highly peaked around the $q = (2m+1)/2n$ surface. Then a simple analytical form for the growth rate of the TAE mode can be obtained by evaluating A_s at this surface:

$$\gamma/\omega_0 \cong \frac{9}{4}\left[\beta_\alpha\left(\frac{\omega_{*,\alpha}}{\omega_0} - \frac{1}{2}\right) F - \beta_e \frac{v_A}{v_e}\right] \tag{31}$$

where the function F is defined as $F(x) = x(1+2x^2+2x^4)e^{-x^2}$. The first term in the square bracket on the right-hand side of Eq. (31) comes from the alpha particles and is destabilizing if $\omega_{*,\alpha}/\omega_0 > 1$, whereas the second term is due to electron Landau damping and is always stabilizing since $|\omega_{*,e}/\omega_0| \ll 1$. Thus we have two conditions for the TAE modes to be unstable. The first condition requires $\omega_{*,\alpha}/\omega_0 > 1$, i.e., that the alpha density scale length is small enough. The second condition requires that the alpha particle destabilization overcomes the electron damping effect. We can balance these two terms by determining the value of L_α that maximizes the growth rate. Calculating $\frac{\partial}{\partial L_\alpha}\left(\frac{\gamma}{\omega_0}\right) = 0$ with the radial profile

for $\beta_\alpha(r)$ given above, for which $\omega_{*\alpha} = m\rho_\alpha v_\alpha / L_\alpha^2$, we find

$$\left(\frac{L_\alpha}{a}\right)_{\max} = \left(\frac{2\delta y^2}{2\delta + y^2}\right)^{1/2} = 0.59 \tag{32}$$

where $y = 1/\sqrt{2}$ is the value of r/a at the point where $q(r) = 1.5$ and $\delta = (L_\alpha/a)^2(\omega_{*\alpha}/\omega_0) = 0.55$. Then we first can calculate the threshold β_α value by setting the maximized growth rate equal to zero:

$$\beta_{\alpha,\mathrm{crit}}(0) = \frac{\beta_e \left(\frac{v_A}{v_e}\right) \exp(ay/L_\alpha)^2}{\left(\frac{\omega_{*\alpha}}{\omega_0} - \frac{1}{2}\right) F} \cong 0.3\% \tag{33}$$

since $F = 1.67$ for $v_A/v_\alpha = \frac{1}{2}\sqrt{3.5}$. Next, we calculate the growth rate well above threshold, at $\beta_\alpha(0) = 3.0\%$ and $L_\alpha/a = 0.59$ (corresponding to the parameters in Fig. 8) and obtain $\gamma/\omega_0 = 2.6 \times 10^{-2}$, which agrees with the numerical result very closely.

4 Study of Toroidicity-Induced Alfvén Eigenmodes with the NOVA Code

In Section 3, the alpha particle destabilization of the TAE mode was described by means of model equilibrium profiles. The same eigenmodes were also self-consistently investigated[9] with the use of numerically computed finite β equilibria with noncircular flux surfaces through the use of a nonvariational kinetic-MHD hybrid code (NOVA-K). Details concerning this code have been described by Cheng.[14,15]

In this approach, the ideal MHD fluid description is adopted for the core plasma (labeled c), with a drift kinetic description for the alpha particles, which are assumed to have low beta but be highly energetic: $\beta_\alpha < \beta_c$, but $T_\alpha \gg T_c$. The alpha particles interact with the core plasma through their perturbed pressure tensor $\delta\mathbf{P}_\alpha$ in the momentum balance equation for the fluid displacement $\boldsymbol{\xi}$:

$$\omega^2 \rho \boldsymbol{\xi} = \nabla \delta P_c + \nabla \cdot (\delta \mathbf{P}_\alpha) + \delta\mathbf{B} \times \mathbf{J} + \mathbf{B} \times \delta\mathbf{J} \ , \tag{34}$$

where $\delta\mathbf{B}$ and $\delta\mathbf{J}$ are the perturbed magnetic field and current. The alpha particle pressure $\delta\mathbf{P}_\alpha$ is obtained from the solution for the alpha particle perturbed distribution function, which incorporates both transit and bounce resonance effects. Core plasma kinetic effects on this mode are neglected here.

The resulting integro-differential eigenmode equations were solved in a general toroidal flux coordinate system for realistic numerical equilibria by means of the NOVA-K code. The alpha particle equilibrium distribution function, $F_{0\alpha}$, was taken to be isotropic in pitch angle Λ and slowing down in energy ε, as follows:

$$F_{0\alpha} = \begin{cases} c(\psi)\varepsilon^{-3/2} & \text{for } \varepsilon < \varepsilon_\alpha \\ 0 & \text{for } \varepsilon < \varepsilon_\alpha \end{cases} . \tag{35}$$

Here ε_α is the alpha particle birth energy, and $c(\psi)$ is proportional to the alpha particle density, which was taken to be functionally related as $c(\psi) \propto [P(\psi)]^{7/2}$ to the total plasma pressure $P(\psi)$.

Figure 9 shows the growth rate for the $n = 1$ fixed boundary TAE mode as a function of the alpha particle diamagnetic drift frequency $\omega_{*\alpha}$ (evaluated at $y^{1/2} = 0.5$ and for $m = 1$) normalized to $\omega_A = V_A(0)/q(a)R$, for a numerical equilibrium with a circular plasma boundary. The pressure profile is $P(y) \propto (1 - y^2)^2$, with $y = \psi/\Delta\psi$ the normalized poloidal flux. The other parameters for Fig. 9 are $q(0) = 1.05$, $q(a) = 2.3$, $R/a = 4$, $\langle\beta_{\text{total}}\rangle = 1.89\%$, and $\langle\beta_\alpha\rangle = 0.4\%$. The real frequency of the mode is $\omega_r/\omega_A = 0.705$, which lies within the continuum gap formed by the toroidal coupling of the $m = 1$ and $m = 2$ modes at $q = 1.5$. The wave functions for the $m = 1$ and $m = 2$ modes show that these modes peak near $y^{1/2} = 0.5$; hence $\omega_{*\alpha}$ is a good measure of the alpha particle free energy that can be accessed through inverse Landau damping. Figure 9 shows that $\omega_{*\alpha}/\omega_A \gtrsim 1.5$ and that beyond this threshold the growth rate γ is approximately linearly proportional to $\omega_{*\alpha}$. From these results we find that for typical ignition parameters, the growth rate of the $n = 1$ TAE mode can be of the order of 10^{-2} of the real frequency. This is roughly one order of magnitude

larger than the GAE mode growth rates (evaluated at small a/R).

The numerical results concerning the global shear Alfvén waves can be interpreted as follows. From the eigenmode equations [cf. Eq. (34)], one can construct the quadratic form

$$\omega^2 \delta K = \delta W_f + \delta W_\alpha \ . \tag{36}$$

Here, δK is the inertial energy, δW_f is the fluid-like potential energy, and δW_α is the potential energy of the kinetic alpha particles (including their transit and bounce resonances). For the mode frequency, we write $\omega = \omega_r + i\gamma$ and assume that the growth rate is small ($|\gamma| \ll |\omega_r|$). Then Eq. (36) yields

$$\gamma \cong -\mathrm{sgn}(\omega_r) \int d\psi d\Lambda \left(\frac{9\pi^2 \widehat{\tau}_t}{4\delta K}\right) P(\psi) \sum_{m,m'p=-\infty}^{\infty} \frac{\left[\omega_r - \omega_{*\alpha}^{(m)} \left(\frac{\omega_r/\omega_t)}{p-nq}\right)^2\right]}{(p-nq)^2 \omega_t^2} \mathrm{Re}\left[\langle G_{m'p}\rangle^* \langle G_{m,p}\rangle\right] \ , \tag{37}$$

where $G_{m,p} = F_m(\Lambda,\theta) \exp\left\{i[(m-nq)\theta - (p-nq)\omega_t \widehat{t}]\right\}$, $F_m(\Lambda,\theta)$ depends on the pitch angle, the equilibrium θ-variation, and the mode amplitude; $\widehat{t}$ is the time-like variable measuring alpha particle position along a field line; ω_t and $\widehat{\tau}_t$ are the alpha particle transit frequency and transit time, respectively; and $\langle G_{m,p}\rangle$ is the transit average of $G_{m,p}$. The transit harmonic number is p, where p values close to m contribute the most. We define $\omega_{*\alpha}^{(m)} = m\omega_{*\alpha}$, where, $\omega_{*\alpha}$ is the diamagnetic frequency for $m = 1$.

Equation (37) shows that the instability condition is $\omega_{*\alpha}^{(m)} \gtrsim \omega_r$; here the alpha particle free energy drive overcomes usual Landau damping. This marginal stability condition agrees with the numerical result, shown in Fig. 9, for which $\omega_{*\alpha}/\omega_A \simeq 1.5$ is marginal. Above this threshold, Eq. (37) indicates that the growth rate γ will tend to scale linearly with $\omega_{*\alpha}$, which again agrees with Fig. 9.

Incidentally, the form of Eq. (37) also shows why the $n = 0$ GAE mode is stable in toroidal geometry. Since the the alpha particle effects are perturbatively small, to a good approximation the mode structure is given by the ideal MHD toroidal wavefunctions. Being self-adjoint, these wavefunctions have the symmetry property $|G_{m,p}|^2 = |G_{-m,-p}|^2$ for $n = 0$.

Thus, the alpha particle excitation terms $\omega_{*\alpha}^{(m)}$ and $\omega_{*\alpha}^{(-m)}$ are seen to tend to cancel in Eq. (37), so that the $n = 0$ GAE mode is stable.

More precisely, Ross[16] has pointed out that this result for the $n = 0$ mode holds when the toroidicity is not too small. After all, in the cylindrical limit, the $n = 0$ mode with single m can be destabilized by transiting alpha particles. Moreover, strictly speaking, the symmetry between the $\pm m$ mode amplitudes is broken by the presence of the $\omega_{*\alpha}$ terms. A simple zero-dimensional mode coupling argument allows an estimate of how large the toroidicity should be to give the stable result that is observed numerically. In general, this estimate indicates that the $n = 0$ mode could be unstable only if $(\gamma_m/\omega_m) > O(\langle\varepsilon\rangle^{m+1})$, where ω_m and γ_m are the real frequency and the cylindrical growth rate due to the alpha particle contribution for the mode $(0, m)$, and $\langle\varepsilon\rangle$ measures the effect of inverse aspect ratio. However, this condition is not satisfied for the typical ignition parameters used in the numerical studies of this paper. In particular, for $m = 1$ and $m = 2$, which are the most unstable modes in the cylindrical limit, we have $\gamma_m/\omega_m \lesssim 10^{-3}$, whereas $\langle\varepsilon\rangle = 0.25$. Therefore the result for the $n = 0$ GAE mode being stable in toroidal geometry is indeed valid.

5 Stability of TAE Modes in ITER

Thus far in our discussion of the destabilizing effect of thermonuclear alpha particles on global-type shear Alfvén modes, we have concluded that the toroidicity-induced Alfvén eigenmodes pose a potential threat to confinement. It is of interest, therefore, to consider what our theory of these modes would predict for the proposed ITER ignition plasma.

We apply the theoretical description of Section 3, assuming the same radial profiles. Also, we take the central value for the alpha particle density to be 2% of the corresponding value for the ion or electron density.

The results for the growth rate γ (including the electron damping contribution) as a

function of the alpha particle density scale length L_α for the $n = 1$ TAE mode are shown in Fig. 10, normalized to the real frequency. We repeated this calculation twice for the two phases of ITER. Thus, the solid curve in Fig. 10 corresponds to the ITER Physics Phase, for which the parameters are $R = 5.8\,\mathrm{m}$, $a = 2.2\,\mathrm{m}$, $B = 5\,\mathrm{T}$, and $n_e = 6 \times 10^{19}\,\mathrm{m}^{-3}$. The dashed curve in Fig. 10, on the other hand, corresponds to the ITER Technical Phase, for which the parameters are $R = 5.5\,\mathrm{m}$, $a = 1.8\,\mathrm{m}$, $B = 5.3\,\mathrm{T}$, and $n_e = 6.7 \times 10^{19}\,\mathrm{m}^{-3}$. The real frequency (normalized to the Alfvén frequency at $q = 1.5$) is 0.90 for the Physics Phase and 0.91 for the Technical Phase.

The interesting result is the $n = 1$ TAE mode is stable for both ITER phases. This can be understood if we note that

$$\frac{\omega_{*\alpha}}{\omega_A} \propto \left(\frac{\rho_{\alpha 0}}{a}\right)\left(\frac{R}{a}\right)\left(\frac{v_{\alpha 0}}{v_A}\right) . \tag{38}$$

Computing the relevant quantities, we find that $R/a = 2.6$, $\rho_{\alpha 0}/a = 0.024$, $v_{\alpha 0}/v_A = 1.5$, $\beta_e(0) = 2.9\%$, and $\beta_\alpha(0) = 1.9\%$ for the ITER Physics Phase. Correspondingly, for the ITER Technical Phase, we have $R/a = 3.1$, $\rho_{\alpha 0}/a = 0.028$, $v_{\alpha 0}/v_A = 1.5$, $\beta_e(0) = 3.2\%$, and $\beta_\alpha(0) = 2.1\%$. A comparison with the parameters used in Section 3 (which correspond to the parameters for an early version of the CIT device) shows that the TAE modes are stable in ITER because of its relatively large size and also its low density.

6 Conclusion

The results described here in seem to indicate that the global Alfvén eigenmodes (GAE) will not be problematic in ignition tokamaks. Toroidicity (and also electron damping through the curvature drift) tends to stabilize the $n \neq 0$ GAE modes for $a/R > 0.1$, and the $n = 0$ GAE mode is stable when the $\pm m$ mode coupling cancellation effect is taken into account.

Therefore, primary attention — especially in experiments — should be focused on the toroidicity-induced shear Alfvén eigenmodes (TAE), which can be strongly destabilized by

alpha particles. Specifically for ITER parameters, however, we find the fortunate result that the $n = 1$ TAE mode is stable, due to the relatively large size and low density of this device. It should be noted that if the edge plasma density value is reduced, the toroidicity-induced mode may possibly resonate with the shear Alfvén continuum near the plasma periphery, an effect which could be stabilizing and should be investigated. Also, we note that a theory for the nonlinear saturation of linearly unstable TAE modes has recently been developed.[17]

Acknowledgments

This work was supported in part by the U.S. Department of Energy Contract No. DE-FG05-80ET-53088 with The University of Texas, by Association Euratom–Confédération Suisse, and by the U.S. Department of Energy Contract No. DE-ACO2-76-CHO3073 with Princeton University.

References

1. A.B. Mikhailovskii, "Thermonuclear 'Drift' Instabilities," Zh. Eksp. Teor. Fiz. **68**, 1772 (1975) [Sov. Phys.-JETP 41, 890 (1975)].

2. M.N. Rosenbluth and P.H. Rutherford, "Excitation of Alfvén Waves by High-Energy Ions in a Tokamak," Phys. Rev. Lett. **34**, 1428 (1975).

3. K.T. Tsang, D.J. Sigmar, and J.C. Whitson, "Destabilitization of Low Mode Number Alfvén Modes in a Tokamak by Energetic or Alpha Particles," Phys. Fluids **24**, 1508 (1981).

4. Y.M. Li, S.M. Mahajan, and D.W. Ross, "Destabilization of Global Alfvén Eigenmodes and Kinetic Alfvén Waves by Alpha Particles in a Tokamak Plasma," Phys. Fluids **30**, 1466 (1987).

5. C.Z. Cheng and M.S. Chance, "Low-n Shear Alfvén Spectra in Axisymmetric Toroidal Plasmas," Phys. Fluids **29**, 3695 (1986).

6. G.Y. Fu, "Topics in Stability and Transport in Tokamak: Dynamic Transition to Second Stabilty with Auxiliary Heating; Stabilty of Global Alfvén Waves in an Ignited Plasma," Ph.D. Thesis, The University of Texas at Austin, Institute for Fusion Studies Report No. 325 (July, 1988).

7. G.Y. Fu and J.W. Van Dam, "Stability of the Global Alfvén Eigenmode in the Presence of Fusion Alpha Particles in an Ignited Tokamak Plasma," Institute for Fusion Studies Report No. 370 (May, 1989), to be published in Phys. Fluids.

8. G.Y. Fu and J.W. Van Dam, "Excitation of Toroidicity-Induced Shear Alfvén Eigenmode by Fusion Alpha Particles in an Ignited Tokamak," Phys. Fluids B **1**, 1949

(1989).

9. C.Z. Cheng, G.Y. Fu, and J.W. Van Dam, "Toroidal Alfvén Wave Stability in Ignited Tokamaks," in *Theory of Fusion Plasmas* (Proceedings of the 1988 Joint Varenna-Lausanne Workshop), edited by J. Vaclavik, F. Troyon, and E. Sindoni (Editrice Compositori/Societa Italiana di Fisica, Bologna, 1989), p. 259.

10. J.W. Van Dam, M.N. Rosenbluth, H.L. Berk, N. Dominguez, G.Y. Fu, X. Llobet, D.W. Ross, D.P. Stotler, D.A. Spong, W.A. Cooper, D.J. Sigmar, D.E. Hastings, J.J. Ramos, H. Naito, T. Todoroki, S.T. Tsai, S.G. Guo, and J.W. Shen, "Effects of Energetic Particles on Tokamak Stability," in *Plasma Physics and Controlled Nuclear Fusion Research 1986* (IAEA, Vienna, 1987), Vol. II, p. 135.

11. D.W. Ross, G.L. Chen, and S.M. Mahajan, "Kinetic Description of Alfvén Wave Heating," Phys. Fluids **25**, 652 (1982).

12. T.H. Stix, "Alfvén Wave Heating," in *Heating in Toroidal Plasmas* (Proceedings of the Second Joint Varenna-Grenoble Symposium), edited by E. Canobbio et al. (CEC, Brussels, 1980), Vol. II, p. 631.

13. C.Z. Cheng, L. Chen, and M.S. Chance, "High-n Ideal and Resistive Shear Alfvén Waves in Tokamaks," Ann. Phys. (N.Y.) **161**, 21 (1984).

14. C.Z. Cheng, "Kinetic-MHD Stability Calculations for Toroidal Plasmas Using the NOVA-K Code," in *Theory of Fusion Plasmas* (Proceedings of the 1987 Workshop), edited by A. Bondeson, E. Sindoni, and F. Troyon (Editrice Compositori/Societa Italiana di Fisica, Bologna, 1988), p. 185.

15. C.Z. Cheng, "Kinetic Extensions of Magnetohydrodynamic Models for Axisymmetric Toroidal Plasmas," Princeton Plasma Physics Laboratory Report No. PPPL-2604

(April, 1989), to be published in Computer Physics Reports.

16. D.W. Ross, private communication (1988).

17. H.L. Berk and B.N. Breizman, "Saturation of a Single Mode Driven by an Energetic Injected Beam III: Alfvén Wave Problem," Institute for Fusion Studies Report No. IFSR-396 (September, 1989), submitted to Phys. Fluids.

Figure Captions

1. Cylindrical shear Alfvén continua for mode numbers $n = 1$ and $m = -1, -2$, and -3.

2. Numerical eigenfunctions for the toroidal GAE mode $(1, -2)$ and the sidebands$(1, -1)$ and $(1, -3)$, with CIT-like ignition parameters, for the inverse aspect ratio $\varepsilon = 0.1$.

3. Numerical eigenfunctions for the sideband $(1, -1)$ of the toroidal GAE mode $(1, -2)$, with ignition parameters, for the inverse aspect ratio values of $\varepsilon = 0.05$, 0.20, 0.30, and 0.48.

4. Electron Landau damping rate γ_L and the total growth rate γ (with alpha particles), as functions of the inverse aspect ratio ε for the toroidal GAE $(1, -2)$ mode coupled to the sidebands $(1, -1)$ and $(1, -3)$.

5. Growth rate γ for the cylindrical GAE mode $(0, -2)$, both with the electron curvature drift term (solid curve) and also without this term (dashed curve), as a function of the alpha particle density scale length L_α, for CIT-like ignition parameters.

6. Toroidal shear Alfvén continuous spectrum with gap, for safety factor profile $q = 1 + (r/a)^2$ and a constant density profile; the cylindrical spectra (dashed curves) for $m = -1$ and $m = -2$, with $n = -1$, cross at the flux surface where $q = 1.5$.

7. Radial profiles of the dominant poloidal harmonics for the $n = -1$ TAE mode as a function of the alpha particle density gradient scale length.

8. Growth rate (normalized to the real frequency ω_r) for the $n = -1$ TAE mode as a function of the alpha particle density gradient scale length for CIT-like ignition parameters.

9. Growth rate γ for the $n = 1$ toroidicity-induced shear Alfvén eigenmode as a function of the alpha particle diamagnetic drift frequency ω_{*_a} (normalized to the shear Alfvén frequency ω_A), as obtained with the NOVA-K code.

10. Growth rate (normalized to the real frequency ω_r) for the $n = -1$ TAE mode as a function of the alpha particle density gradient scale length for ITER parameters corresponding to the ITER Physics Phase (solid curve) and Technical Phase (dashed curve).

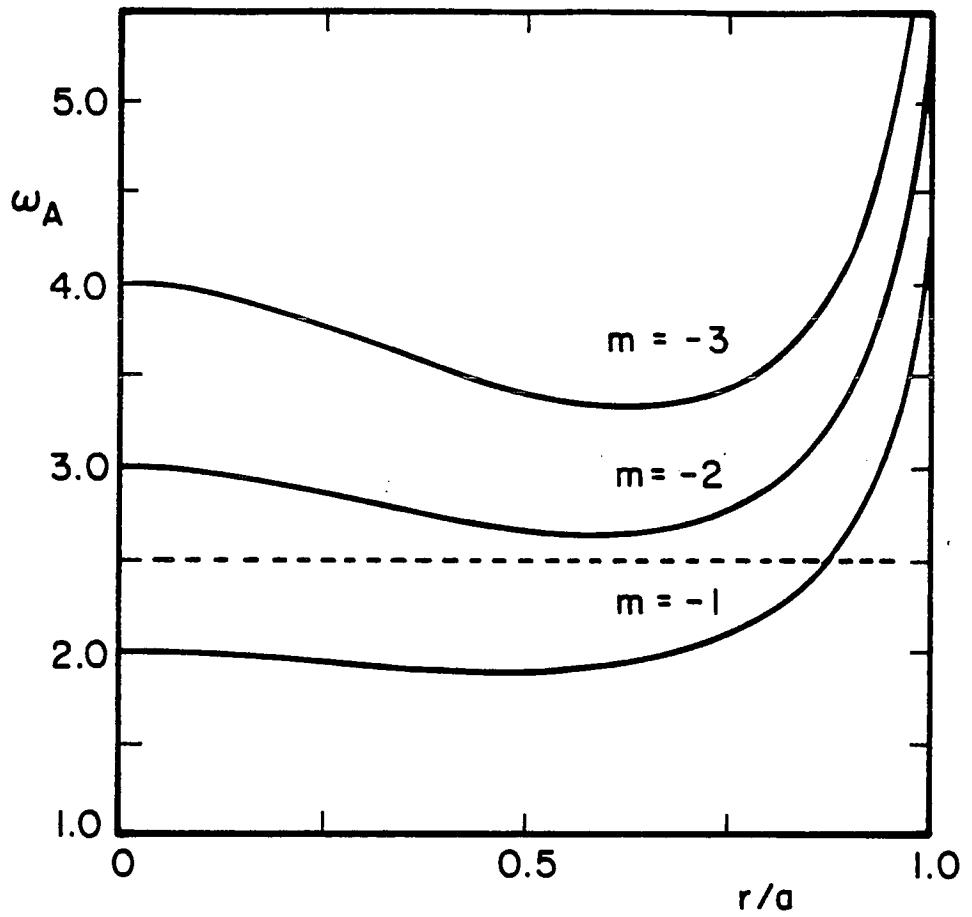

Figure 1

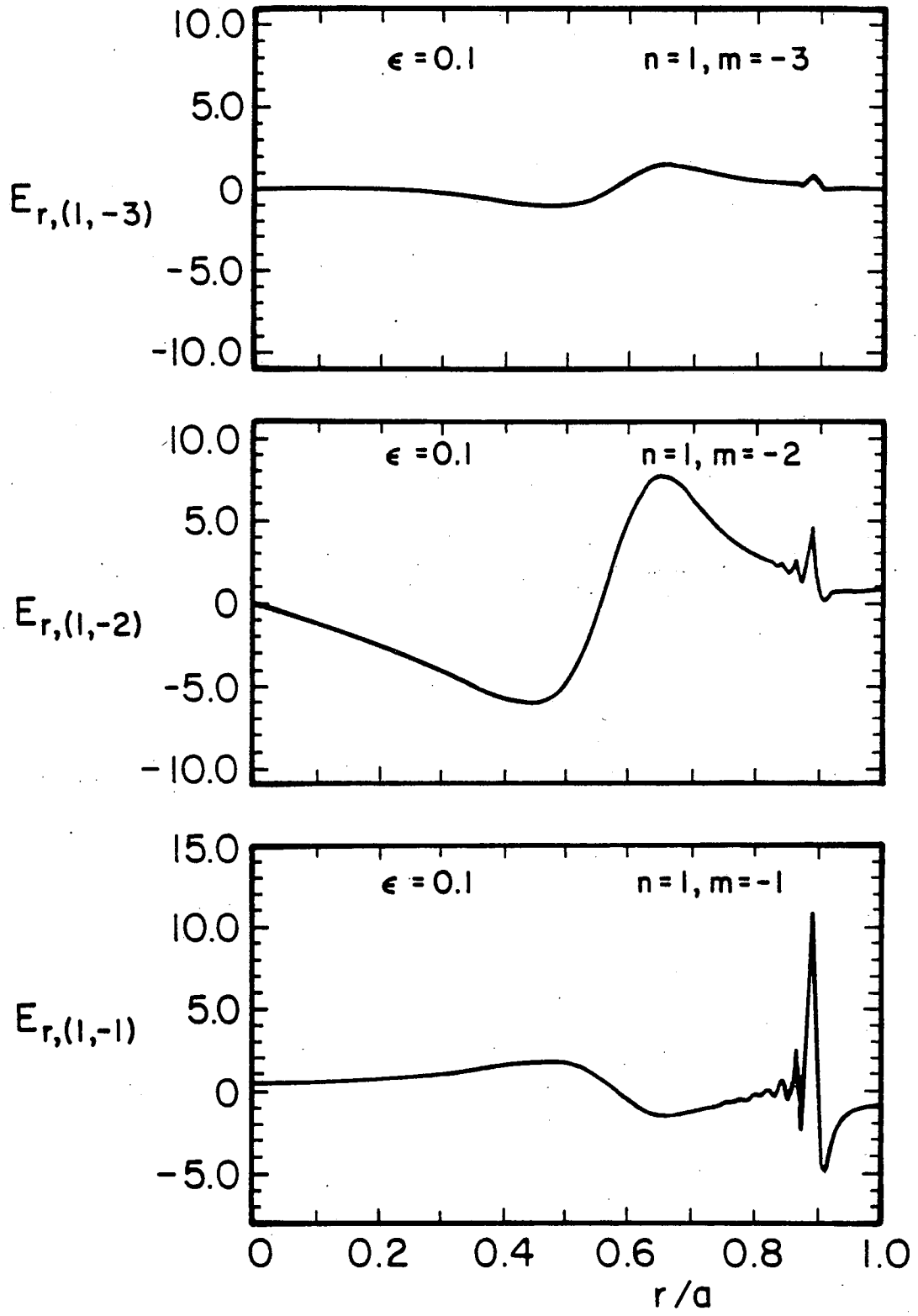
10.0
5.0
0
-5.0
-10.0
ϵ = 0.1
n = 1, m = -3
$E_{r,(1,-3)}$
10.0
5.0
0
-5.0
-10.0
ϵ = 0.1
n = 1, m = -2
$E_{r,(1,-2)}$
15.0
10.0
5.0
0
-5.0
ϵ = 0.1
n = 1, m = -1
$E_{r,(1,-1)}$
0
0.2
0.4
0.6
0.8
1.0
r/a

Figure 2

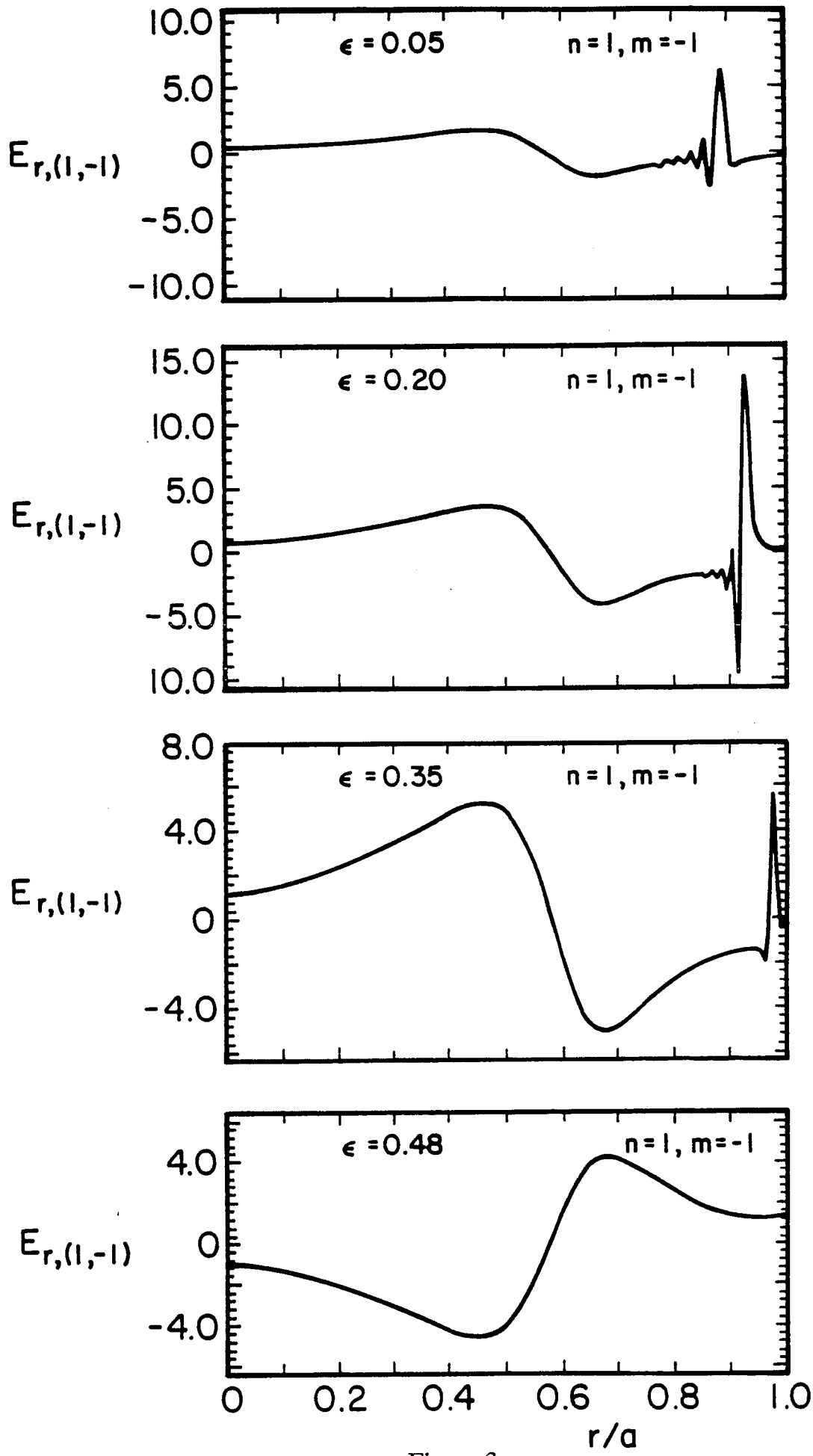
10.0
5.0
0
-5.0
-10.0
ε = 0.05
n = 1, m = -1
E r,(1,-1)
15.0
10.0
5.0
0
-5.0
10.0
ε = 0.20
n = 1, m = -1
E r,(1,-1)
8.0
4.0
0
-4.0
ε = 0.35
n = 1, m = -1
E r,(1,-1)
4.0
0
-4.0
ε = 0.48
n = 1, m = -1
E r,(1,-1)
0
0.2
0.4
0.6
0.8
1.0
r/a

Figure 3

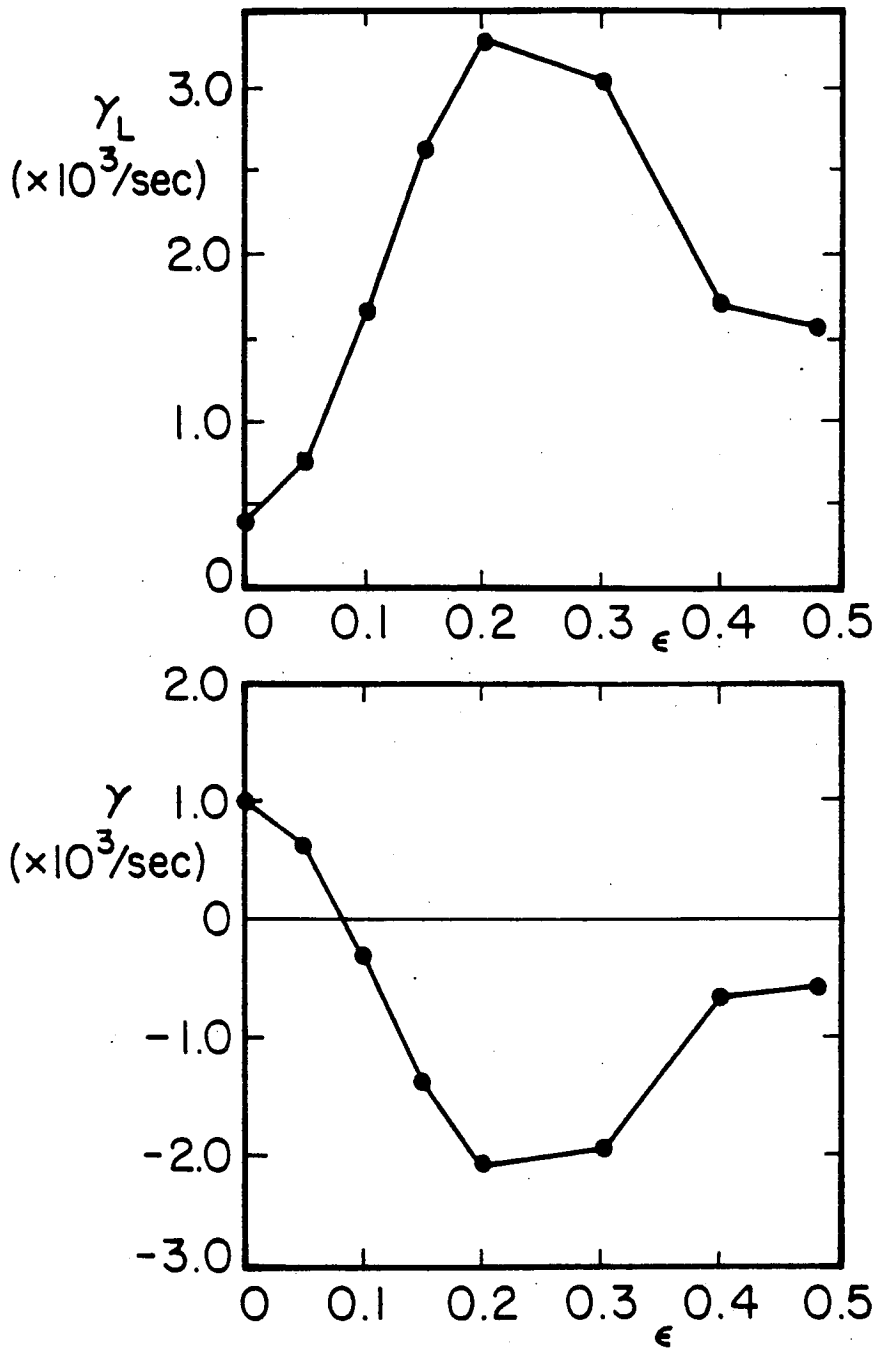
γ_L
(×10³/sec)
3.0
2.0
1.0
0
0
0.1
0.2
0.3
ϵ
0.4
0.5
2.0
γ 1.0
(×10³/sec)
0
-1.0
-2.0
-3.0
0
0.1
0.2
0.3
ϵ
0.4
0.5

Figure 4

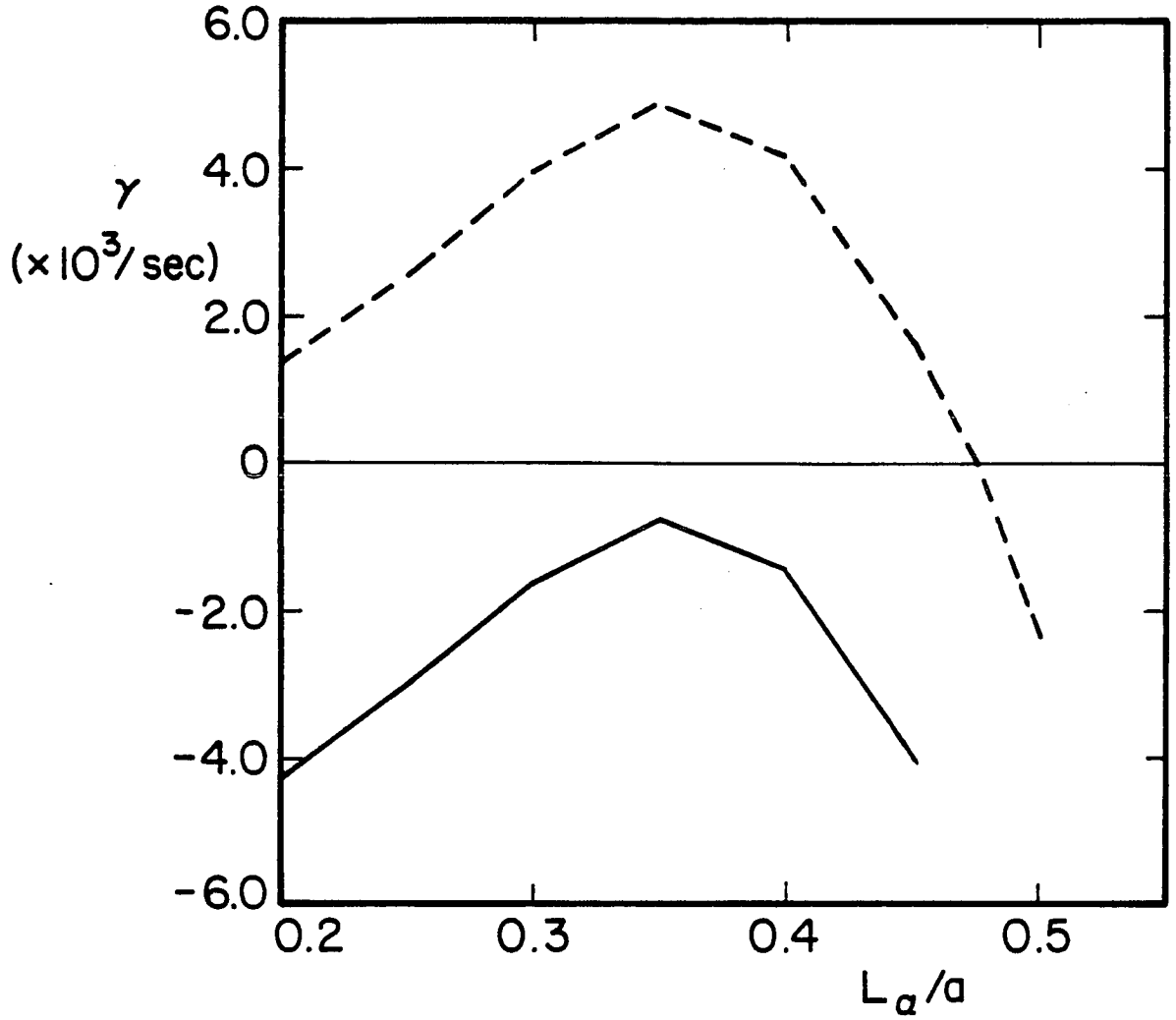

Figure 5

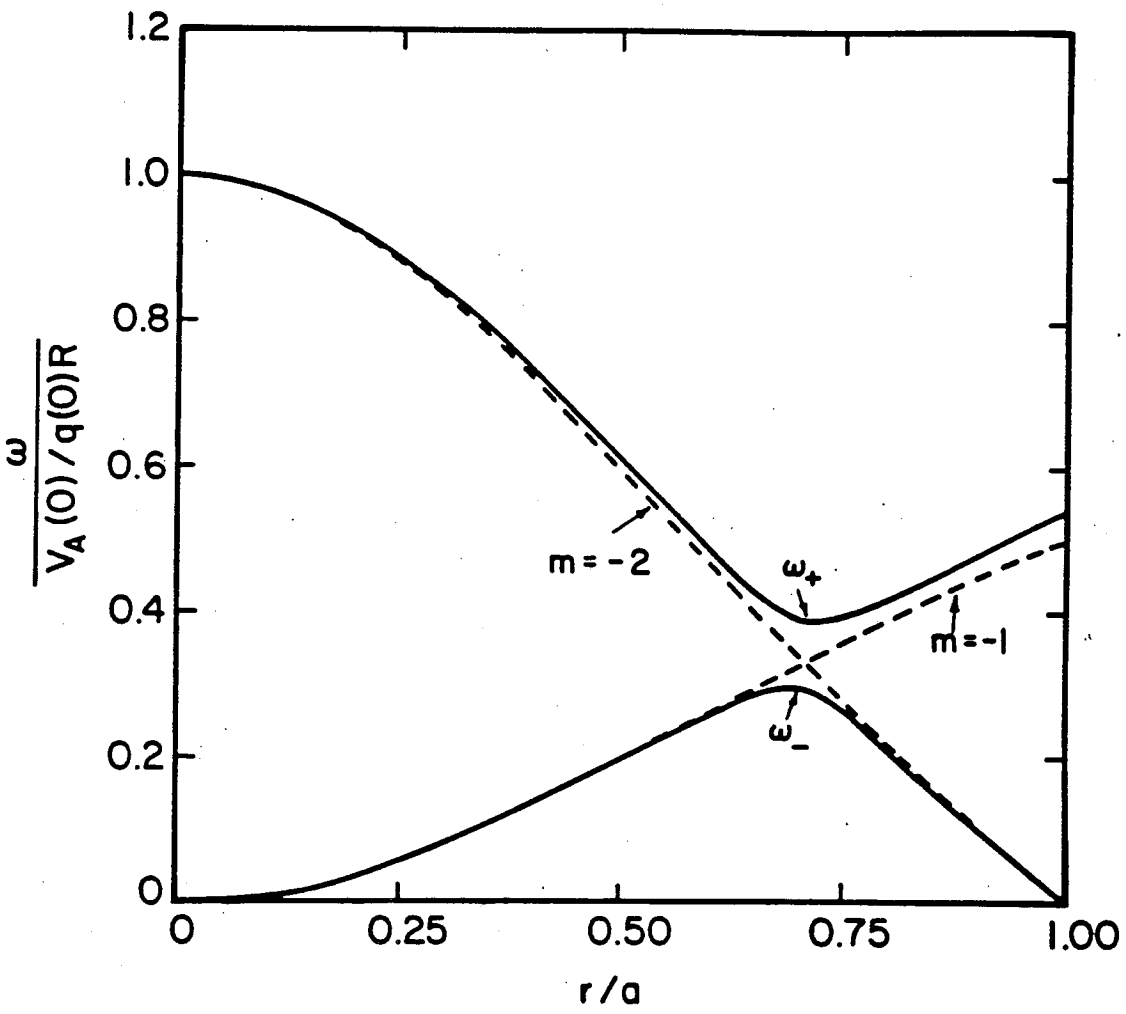

Figure 6

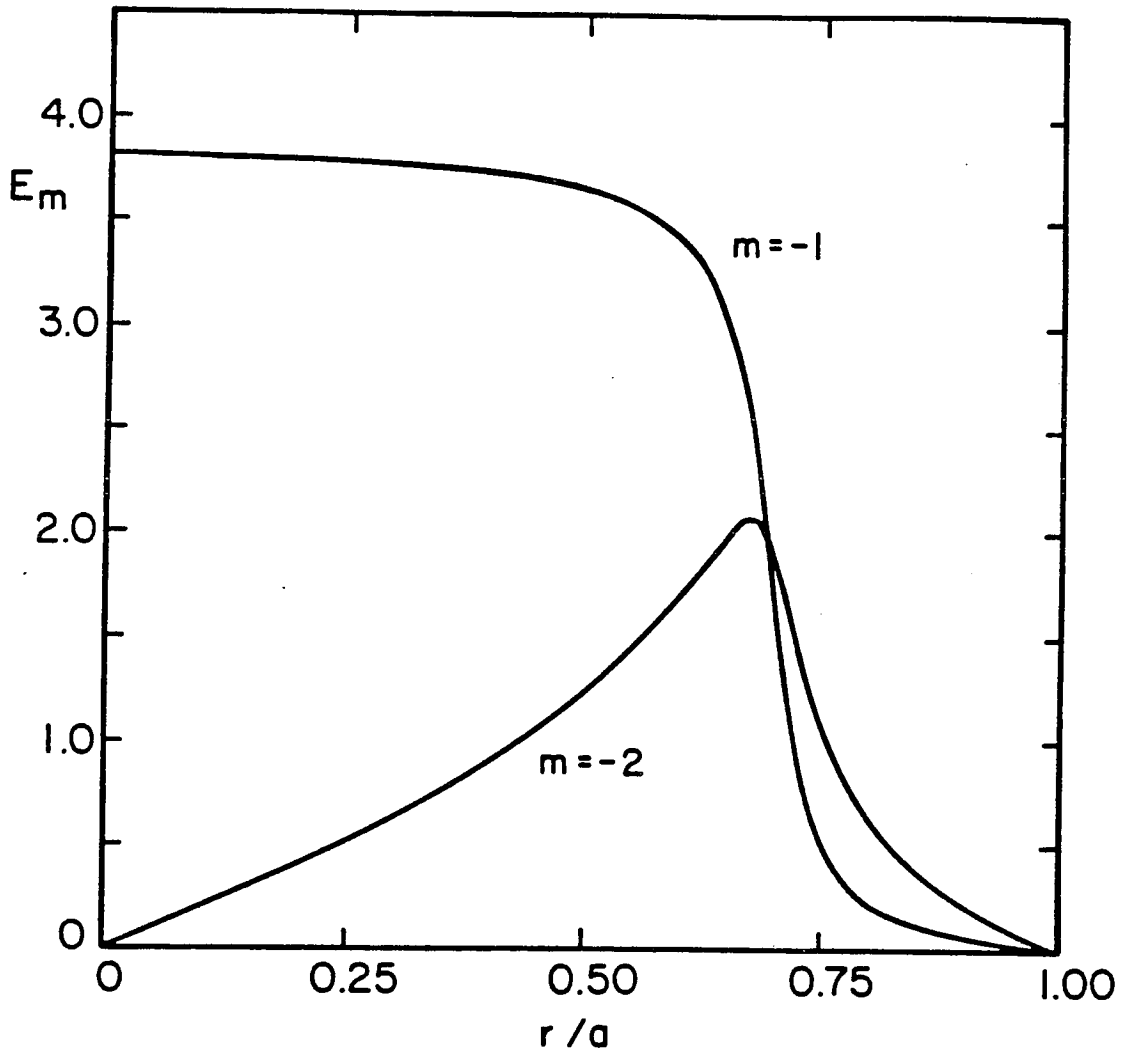

Figure 7

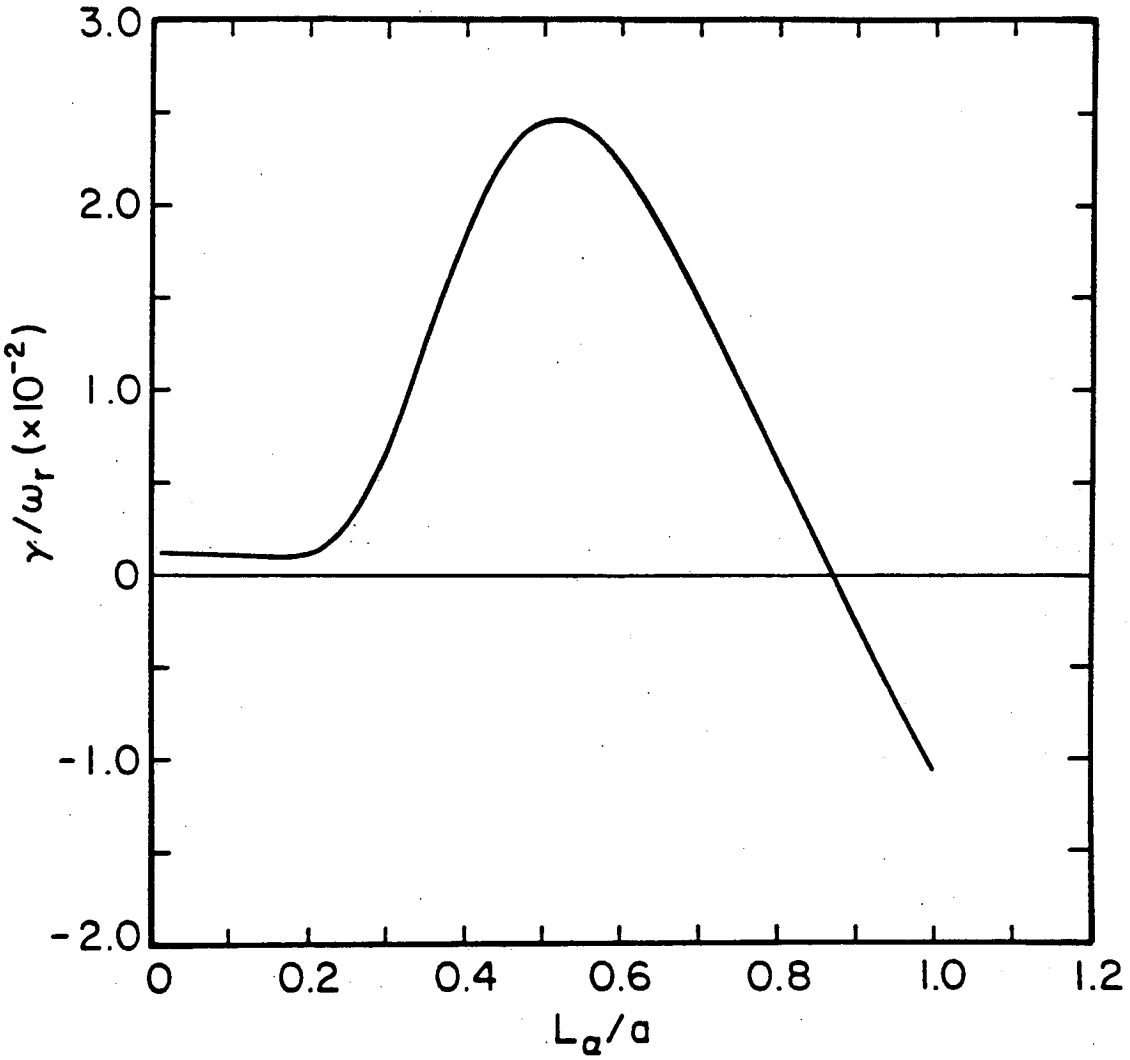
3.0
2.0
1.0
0
-1.0
-2.0
γ/ω_r ($\times 10^{-2}$)
0
0.2
0.4
0.6
0.8
1.0
1.2
L_α/a

Figure 8

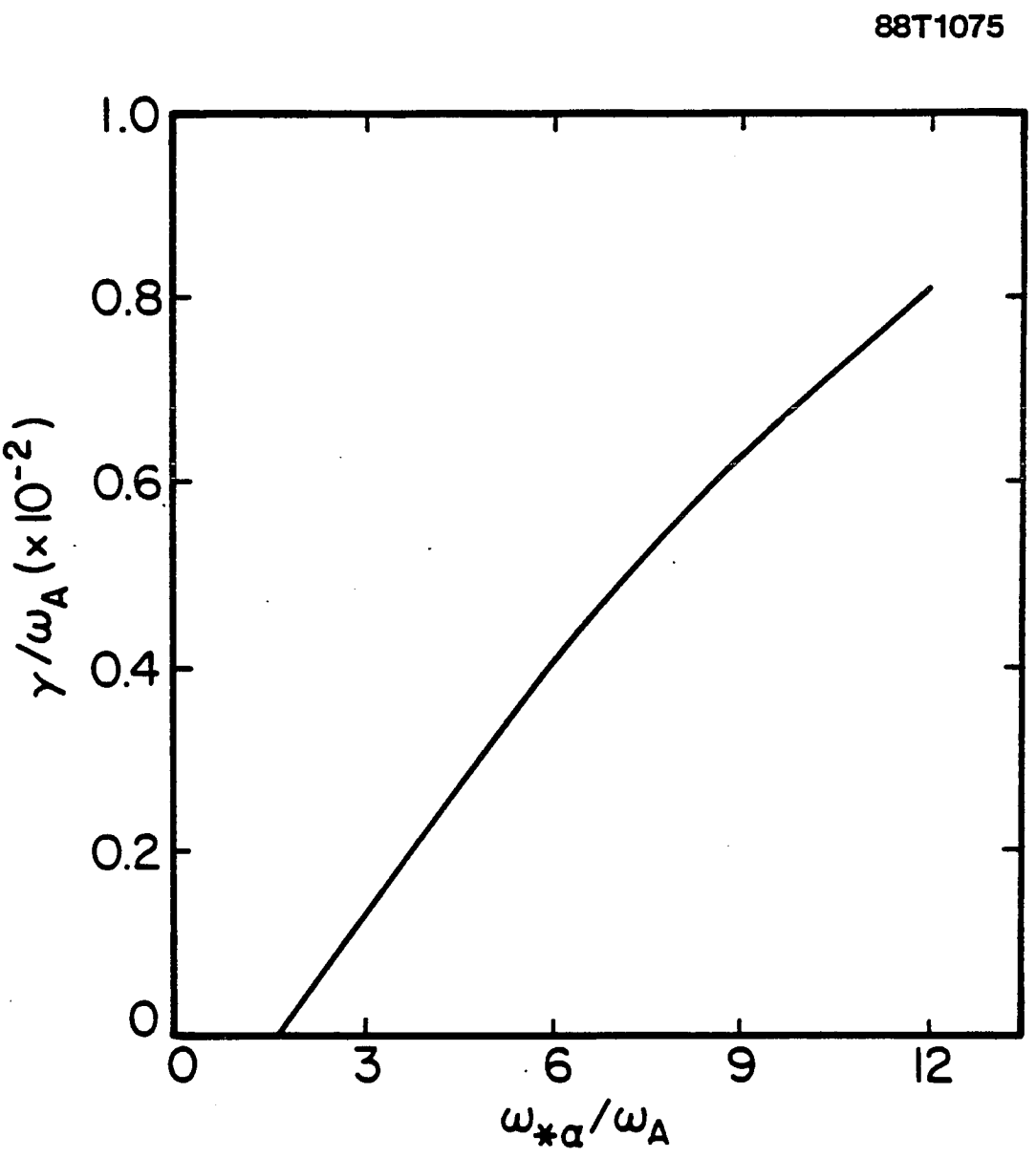
88T1075
1.0
0.8
0.6
0.4
0.2
0
γ/ω_A ($\times 10^{-2}$)
0
3
6
9
12
$\omega_{*\alpha}/\omega_A$

Figure 9

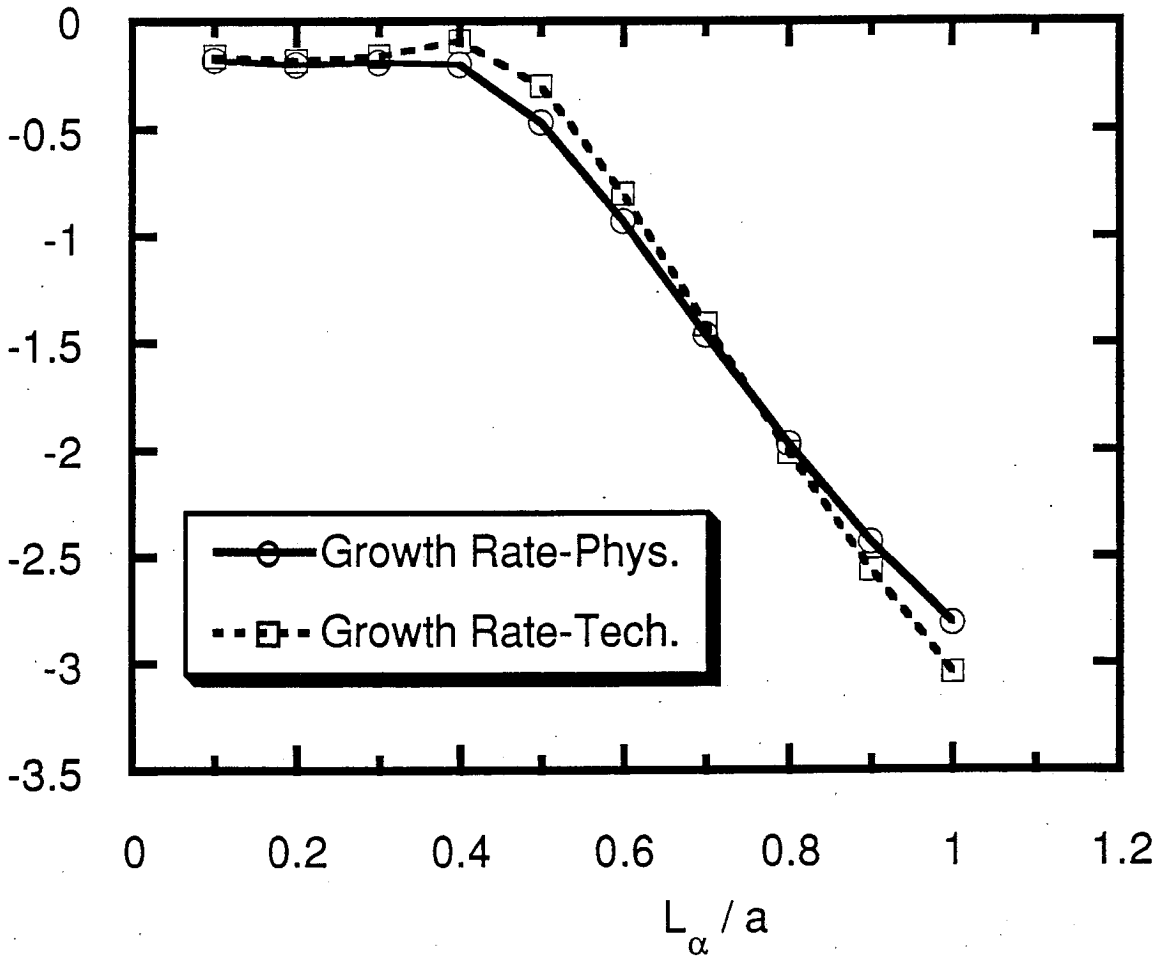
0
-0.5
-1
-1.5
-2
-2.5
-3
-3.5
0
0.2
0.4
0.6
0.8
1
1.2
Growth Rate-Phys.
Growth Rate-Tech.
L_α / a

Figure 10